IAC-08-D2.3.9

A CONCEPT FOR THE ENTRY, DESCENT, AND LANDING OF HIGH-MASS PAYLOADS AT MARS

Ashley M. Korzun, Gregory F. Dubos, Curtis K. Iwata
Georgia Institute of Technology, United States
akorzun@gatech.edu, greg.dubos@gatech.edu, cukii@gatech.edu

Benjamin A. Stahl
NASA Johnson Space Center, United States
benjamin.a.stahl@nasa.gov

John J. Quicksall
Jet Propulsion Laboratory, United States
jakequicksall@yahoo.com

ABSTRACT

The architecture concepts and aggressive science objectives for the next phases of Mars exploration will require landed masses an order of magnitude or greater than any Mars mission previously planned or flown. Additional studies have shown the requirements for missions more ambitious than the 2009 Mars Science Laboratory (~ 900 kg payload mass) to extend beyond the capabilities of Viking-heritage entry, descent, and landing (EDL) technologies, namely blunt-body aeroshells, supersonic disk-gap-band parachutes, and existing TPS materials. This study details a concept for Mars entry, descent, and landing capable of delivering a 20 t payload within 1 km of a target landing site at 0 km MOLA. The concept presented here explores potentially enabling EDL technologies for the continued robotic and eventual human exploration of Mars, moving beyond the Viking-heritage systems relied upon for the past 30 years of Mars exploration. These technologies address the challenges of hypersonic guidance, supersonic deceleration, precision landing, and surface hazard avoidance. Without support for the development of these enabling technologies in the near term, the timeline for the successful advanced exploration of Mars will likely extend indefinitely.

INTRODUCTION

Mars surface missions present a unique set of challenges to EDL designers. The atmosphere is too thin to provide appreciable deceleration yet sufficiently dense to generate substantial aerodynamic heating. Topographic variability heightens the need for robust surface hazard avoidance during terminal descent and precision landing. Flight qualification presents an additional challenge, as ground test facilities cannot fully simulate Mars entry conditions. The maturation of new EDL technologies is likely to require a development effort similar to the cost-intensive Viking qualification programs of the 1970s.

The 2009 Mars Science Laboratory (MSL) mission, with a payload of approximately 900 kg to land at +1 km MOLA within a 12.5 km landing footprint, is challenging the capabilities of Viking-heritage EDL technologies, defining an upper bound on the performance of existing systems [1]. NASA studies have concluded that existing EDL technologies, including blunt-body aeroshells, supersonic disk-gap-band (DGB) parachutes, and existing TPS materials, lack the capability to enable lander missions with requirements extending beyond those for MSL [2]. These heavy-payload missions require parachute diameters exceeding 30 m with deployment above Mach 2.7, conditions exceeding the qualifications developed through the expensive Viking BLDT program [1]. Additionally, the heat rates from the increased ballistic coefficients of these entry vehicles exceed the qualifications of existing TPS materials including SLA-561V and PICA [2]. The capabilities of Viking-heritage EDL technologies, systems which have performed so successfully over the past 30 years with only incremental improvements in performance, have been pushed to their limits by MSL and will be unable to support the next tier of Mars surface exploration.

Past missions have been limited by heritage EDL systems to the lower, less rugged equatorial elevations. Scientifically promising landing sites have been proposed in the highlands, away from the equator, presenting a need for more capable EDL technologies. To safely land in these higher regions or to land multiple payloads for a Martian outpost, the landing footprints of

these systems must be reduced by at least an order of magnitude from MSL.

This study describes an architecture capable of landing a 20 t payload on Mars at 0 km MOLA in the northern hemisphere, with payload defined as the usable portion of the landed mass. The payload is delivered to within 1 km of a predefined landing site, reaching the target with a minimum 99% probability. The concept presented here focuses on the challenges of the thin, but appreciable Martian atmosphere, rugged surface topography, extensive cost of developing new EDL technologies, and the inability to fully test in ground facilities. The limitations of Viking-heritage EDL systems are addressed in this study by utilizing technologies currently under development, including aerocapture, inflatable aerodynamic decelerators (IADs), supersonic retropropulsion, and hypersonic and terminal guidance to achieve the given payload and landing accuracy constraints.

CHALLENGES OF MARS ENTRY, DESCENT, AND LANDING

Atmosphere

The Martian atmosphere presents a unique and complex set of challenges to EDL designers. With only about 1% of the density of Earth's atmosphere, supersonic decelerators are required to slow entering bodies to subsonic terminal descent speeds. However, the atmosphere is still thick enough to generate significant aerodynamic heating, requiring high performance heatshields on entry bodies. Variability of the atmosphere with season, storms, and dust concentrations is difficult to predict and prevents the design of a standard EDL system [1].

Timeline

The low density of the atmosphere causes entering vehicles to fly the hypersonic portion of their trajectories at lower altitudes, severely limiting the amount of time available to transition from a hypersonic entry vehicle to a subsonic terminal lander. This timeline is challenged further as the desired landing site elevation increases. Thus, for a given ballistic coefficient (ratio of entry mass to hypersonic drag area), there is a maximum elevation that can be reached for a prescribed trajectory. Conversely, for example, a 0 km MOLA landing site elevation constrains the ballistic coefficient to be no greater than 135 kg/m^2 using Viking-heritage EDL technologies [1].

Heating

The atmospheric density is sufficient enough to require the entry vehicle to have a forebody TPS, or heatshield. The Viking-heritage TPS material is SLA-561V, a rigid, ablator flown on all 6 successful Mars EDL missions to date. With the increasing ballistic coefficients of future missions, the lower altitudes at which peak deceleration and peak heating occur will demand higher performance TPS.

Surface Topography

The rugged and variable terrain is an additional challenge to EDL designers. Heritage landing systems including crushable legs and airbags are not tolerant of rocks, craters, sloped ground, or uncertain descent conditions. With the Mars Reconnaissance Orbiter, hazards greater than 0.5 m can now be imaged from orbit, though rocks smaller than this can cause a failed landing attempt. The variable terrain can also fool radar altimetry systems, causing premature deployment of drag devices or initiation of terminal descent too soon. MSL will utilize a skycrane to avoid ground interference from the descent engines, allowing the rover to be placed directly on the surface [1]. This system has no direct heritage, but once flown, the skycrane may be a solution for placing larger payloads directly on the surface with a limited capability for hazard avoidance.

Landed Accuracy

With scientifically interesting landing sites predominantly in regions of rocks, craters, and exposed geologic features, the ability of an EDL system to deliver the payload as close to the target as possible becomes critical to the success of the mission. MSL has a target error ellipse of 10 km, a significant improvement in accuracy over the 40 km footprint for the Mars Exploration Rovers (MER). The landed accuracy demands for missions dependent on pre-positioned robotic assets or existing surface infrastructure are up to four orders of magnitude greater than the requirements for MSL [1].

Knowledge and control uncertainty both contribute to the actual miss distance from the target [3], though the relative importance of each of these uncertainties varies during the different phases of the trajectory. Knowledge uncertainty at entry can be reduced to 3 km by using Doppler range and delta-DOR measurements. Use of star trackers and inertial measurement units (IMUs) can reduce the attitude knowledge uncertainty up to 0.5° [4]. Density variations in the atmosphere are also a source of uncertainty in geometric altitude, causing errors on the order of 3 km. With limited data on the wind distribution with altitude, latitude, and season, uncertainty in the wind velocity remains the largest source of error at terminal descent. Surface winds do not generally exceed 20 m/s in the nominal case. However, these winds can exceed 120 m/s at higher altitudes [5]. As a result, guidance capabilities need to be developed for terminal descent to correct for surface winds, especially if the payload is descending on a large, inflatable drag device. Active hypersonic

guidance needs to be developed to correct for higher altitude dispersions, since small errors early in the trajectory can translate into large downrange errors at the surface.

Ability to Qualify and Test New EDL Technologies

The expense of the testing and qualification program for Viking has resulted in no comparable technology development programs being attempted since. Many of the proposed solutions to the Mars heavy-payload EDL problem are technologies in early stages of development, with limited testing or computational simulation completed. Ground facilities are unable to simulate the exact conditions of a Mars entry, preventing full testing of systems such as TPS, aerodynamic decelerators, and aeroshell geometries before flight [1]. These limitations will make the full-scale testing and flight qualification of new EDL technologies difficult, resulting in missions flying with increased risk of an EDL system failure.

NOMINAL VEHICLE CONCEPT

Entry Vehicle Configuration

The entry vehicle configuration is given in Figure 1. The aeroshell is a 70º sphere-cone (12 m diameter) with a ballistic coefficient of 390.3 kg/m^2. The payload is surrounded by six LOX/CH_4 engines used for supersonic propulsive deceleration and terminal descent. Two additional LOX/CH_4 engines are on the vehicle aftbody for on-orbit velocity changes. Eight RCS thrusters are on the aft perimeter of the backshell for attitude adjustments on orbit and during terminal descent. The fuel and oxidizer tanks are above the payload, surrounding the skycrane bridle container. A 30 m diameter IAD is packaged around the vehicle shoulder. A CG offset mass is installed on the entry heatshield to stabilize the vehicle at a trim angle of attack of approximately 11°. The CG offset mass also increases the ballistic coefficient of the heatshield, ensuring the heatshield does not recontact the entry vehicle after jettison. Pallet lander legs are stored in a folded configuration. A detailed mass breakdown is given in Table 1.

EDL Timeline

The nominal trajectory is an aerocapture into low Mars orbit followed by a lifting, guided entry. An IAD deployed at Mach 5 and supersonic retropropulsion initiated at Mach 2 decelerate the vehicle to subsonic conditions. Subsonic terminal propulsion and a skycrane deliver the payload to the surface. A detailed event timeline is given in Figure 2 and continues in Figure 3.

The vehicle approaches Mars on a hyperbolic trajectory with an excess speed of 3.32 km/s. At the beginning of the aerocapture maneuver, the vehicle is traveling 5.94 km/s, entering the atmosphere with a nominal flight path angle of 9.57°. The lift up and lift down entry flight path angles resulting in a desirable post-aerocapture altitude are 9.96° and 8.27° respectively, bounding the allowable error in entry flight path angle for the incoming hyperbolic trajectory. Banked at 45°, the vehicle passes through the atmosphere and dips to a minimum altitude near 30 km. During aerocapture, the peak stagnation point heat rate is approximately 50 W/cm^2, and the integrated heat load is 5300 J/cm^2. The stagnation point heating is used purely to provide a basis for comparison between the trajectories.

Prior to the on-orbit circularization burn, the vehicle is pitched nose up and the aerocapture heat shield is jettisoned. The vehicle is then pitched nose down and performs a circularization burn to place the vehicle in a nominal 200 km orbit. The circularization maneuver requires a ΔV of 110 m/s.

Once in orbit, the vehicle performs any necessary systems checks and acquires the current atmospheric conditions. Following check out, the vehicle deorbits with a ΔV of 110 m/s. While a larger deorbit ΔV would place the vehicle on a steeper entry, a smaller ΔV was chosen to reduce both propellant and TPS mass. Dispersion analyses demonstrate that the shallower flight path angle does not negatively impact the magnitude of trajectory downrange errors with the implementation of hypersonic and terminal guidance.

At the atmospheric interface (defined at 120 km altitude), the vehicle is traveling approximately 3.4 km/s, with an entry flight path angle of -2.7°. The nominal 45° bank angle was chosen to maximize the control authority of the vehicle throughout the entry. In a low energy scenario, the vehicle can bank to a full lift-up trajectory to maximize vertical L/D. Alternatively, downrange travel can be minimized by banking down to 90°. Nominal bank angles higher than 90° result in vehicle impact with the surface. For maximum control authority in cases of dispersed atmospheric and entry conditions, the entry is performed at a nominal bank angle of 45°, allowing for up to 45° of bank angle modulation during hypersonic guided entry.

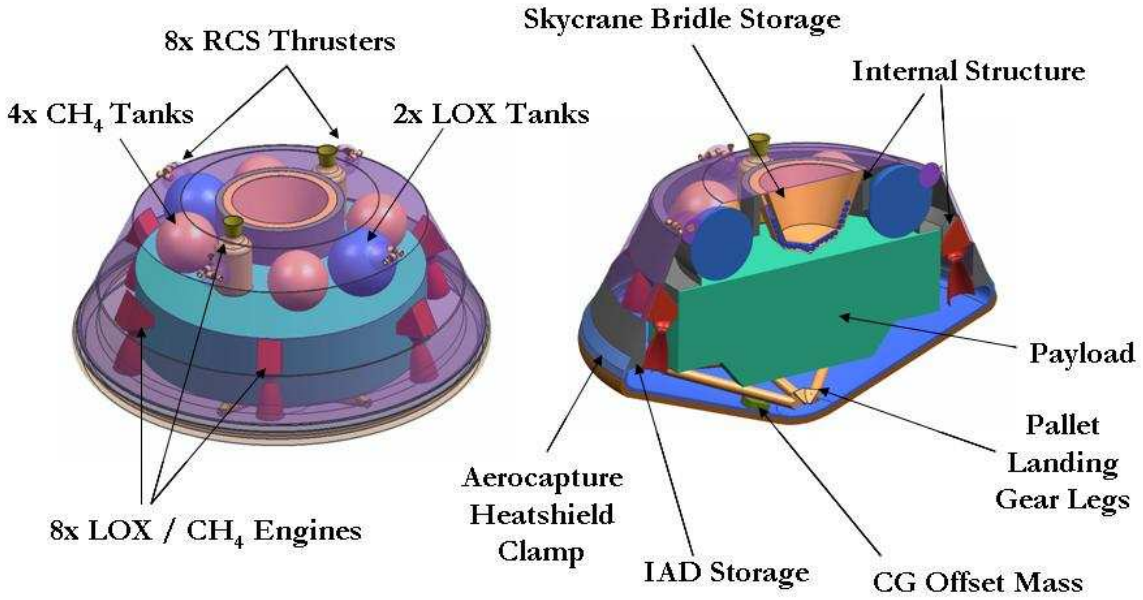

Figure 1: Entry Vehicle Configuration

Table 1: Entry Vehicle Mass Breakdown

	Mass (kg)	Mass Fraction		Mass (kg)	Mass Fraction
Pre-Aerocapture			**Landed Mass**		
TPS (Aerocapture)	5862	9.00%	Payload	20000	30.00%
Propellant	4506	6.92%	Power	1172	1.80%
Sub-Total	10368		Avionics & Comm.	521	0.80%
			Structure (Primary)	8142	12.50%
Post-Aerocapture			Landing Gear	782	1.20%
Propulsion		12.23%	**Sub-Total**	30617	
Engines & Lines	1254				
Propellant	6561		**Dry Mass**	46280	
Tanks	148		**Propellant Mass**	19113	
OMS / RCS	1693	2.60%			
IAD	2147	3.60%	**Margin**		
Terminal Descent		12.35%	Dry Mass (20%)	9256	
Propellant	8046		Propellant Mass (15%)	2867	
TPS (Entry)	4559	7.00%			
Sub-Total	24409		**Total**	**77516**	100.00%

The guided hypersonic phase ends with the deployment of a 30 m diameter IAD at Mach 5, resuming a ballistic trajectory. IAD deployment occurs at an altitude of approximately 12.3 km, with peak loading occurring shortly after deployment (4.5 Earth g's). To deploy the IAD, the IAD storage doors mounted on the lower portion of the backshell open, and the torus is simultaneously inflated with gas generators. In 30 seconds, the IAD decelerates the vehicle to Mach 2 at an altitude of 7.9 km. A second, less massive heatshield is used for the entry and is jettisoned with supersonic retropropulsion initiation at Mach 2. Peak heating occurs much earlier (around Mach 15), and the heating below Mach 2 is negligible. Therefore, jettisoning the second heatshield does not adversely affect heating and improves the trajectory by reducing the vehicle ballistic coefficient. Supersonic retropropulsion provides continuous deceleration until terminal descent guidance takes over at Mach 0.9, approximately 30 seconds later. The nominal downrange traveled from the entry interface to terminal descent guidance engage is 1950 km. The full deceleration profile is given in Figure 4, with the entry phase plotted against entry time t_{entry} and the aerocapture phase against aerocapture time, t_{aero} .

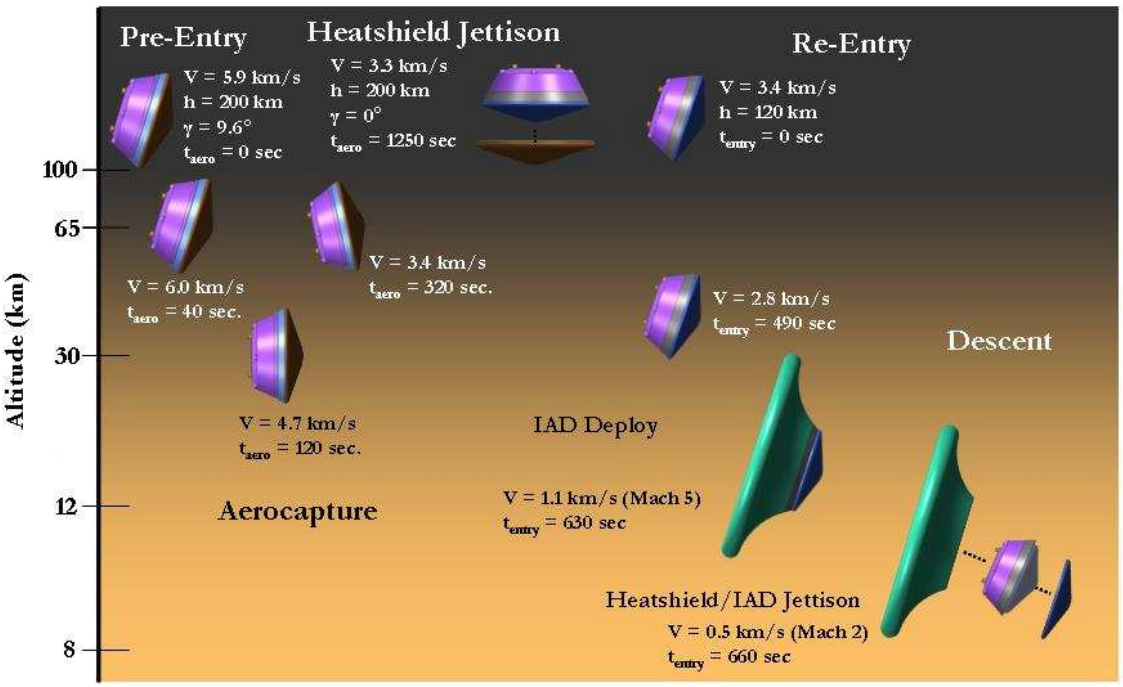

Figure 2: Nominal Aerocapture and Entry Sequence Timeline

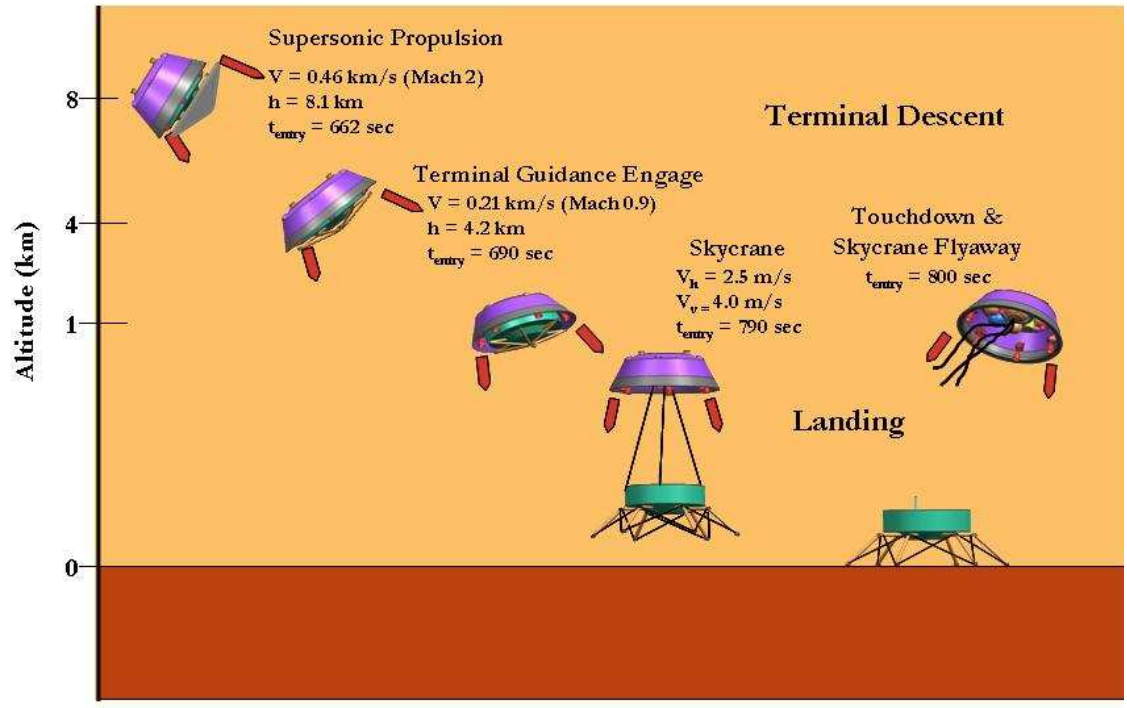

Figure 3: Nominal Descent and Landing Sequence Timeline

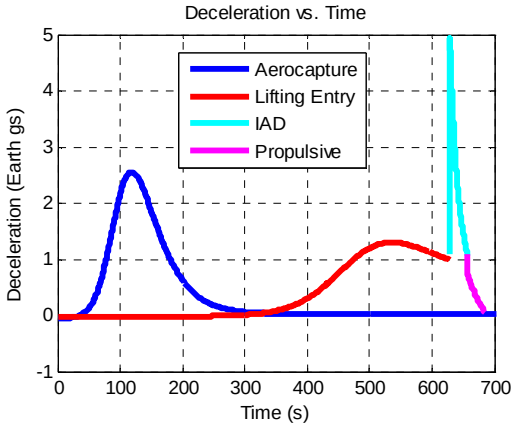

Figure 4: Baseline Deceleration Profile

During terminal descent, the vehicle is propulsively maneuvered, correcting for downrange and crossrange errors from atmospheric variability and winds. At 30 m above the surface, the payload separates from the backshell, deploys the pallet lander legs, and is lowered to the surface at a constant rate of 2.4 m/s, using the 6 engines in the backshell to maintain a position 30 m above the surface. The pallet lander legs are deployed for stability, hazard protection, and shock attenuation as the vehicle reaches the surface. Upon touchdown, the bridle lines are cut, and the skycrane burns the remaining propellant to crash at a safe distance away from the payload landing site.

Landing Site Selection

A minimum altitude of 0 km MOLA and location in the northern hemisphere were used to select the nominal landing site. Locations satisfying these criteria were visually inspected for craters, smoothness, and elevation gradient, with several potential landing sites identified, circled in Figure 5. To minimize the propellant mass required for the plane change maneuvers required to reach higher latitudes, landing sites closer to the equator were given preference. The most easterly landing site, a region of high geologic activity, was selected as the target landing site, indicated in Figure 5 by the solid black ellipse. This site also removes the potential of obstruction on a posigrade entry, since the surface elevation decreases to the east. The coordinates for the nominal target are 11°N, -65°E.

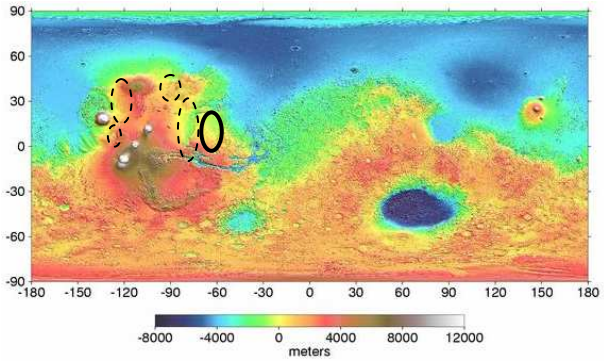

Figure 5: Topographic Map Showing Candidate Landing Sites (MOLA) [6]

EDL ELEMENT OVERVIEW AND TRADE STUDY SUMMARY

Entry Trajectory

Varying the type of entry trajectory results in significant variations in the masses of the TPS, decelerators, propellant, and structure required. To compare a direct ballistic entry, a direct lifting entry, and aerocapture with a lifting entry from low Mars orbit, the vehicle was assumed to be a 10 m diameter 70° sphere cone with a mass of 80 t. The maximum L/D for this geometry is 0.2, with a hypersonic C_D of 1.7 [8]. The velocity profiles for the three entry types are compared in Figure 6. The benefits of aerocapture and a direct lifting entry can be seen in these profiles; the vehicle is decelerated higher in the atmosphere, resulting in velocities of ~1 km/s at altitudes above 5 km. In contrast, the ballistic entry is not able to sufficiently decelerate the vehicle, resulting in velocities near 3.5 km/s at 5 km MOLA.

The corresponding deceleration and convective stagnation point heating profiles are given in Figure 7. The maximum sensed acceleration during aerocapture and the subsequent entry is 2.6 Earth g's, while the peak decelerations for the ballistic and lifting direct entries are 10.5 and 8.4 Earth g's, respectively. Extensibility of this concept to a mission where acceleration limits are fixed and the ability to wait in orbit for favorable atmospheric conditions support the selection of aerocapture over a direct entry.

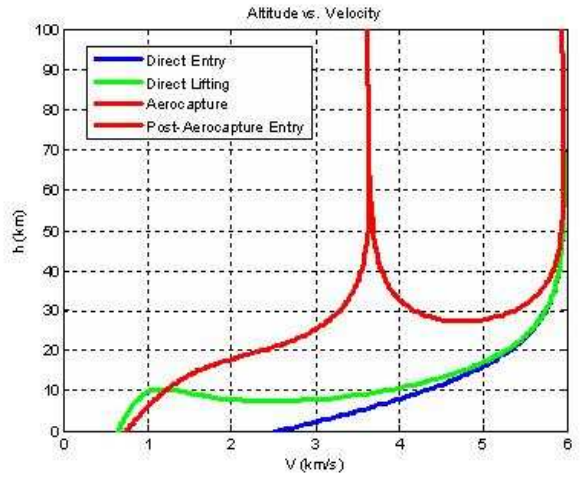

Figure 6: Velocity Profile Comparisons

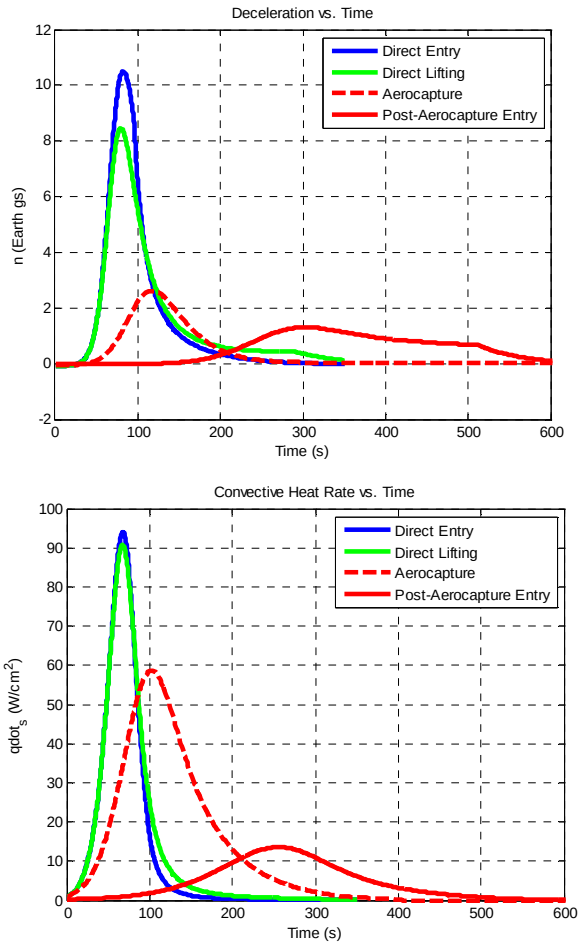

Figure 7: Entry Method Performance Comparison

While aerocapture results in a lower peak heat rate, the total integrated heat load is similar for all three entry types considered. This study baselines aerocapture followed by a lifting entry from a parking orbit over a direct entry, taking advantage of the increased timeline, lower peak deceleration, lower convective stagnation point heat rate, and ability to enter from a parking orbit. While aerocapture has yet to be demonstrated, it was originally planned for Mars Odyssey and could be demonstrated by an upcoming Mars satellite or probe mission of much smaller mass than considered in this study.

Aeroshell Geometry

The baseline aeroshell geometry is the 70º sphere cone, a shape flown on all 6 successful Mars lander missions and will be flown for MSL [1]. Arguments for using heritage systems where possible and study results requiring 10-15% higher entry masses for non-blunt-body aeroshell geometries such as ellipsleds and biconics motivated the selection of the 70º sphere cone [2]. The low L/D of this geometry (L/D = 0.2) was not found to detract from the overall system performance enough to recommend qualifying an entirely new aeroshell geometry with a higher L/D.

A fixed packing density of 150 kg/m^3, based on historical data, was used to size the aeroshell. As the required system mass increased, the aeroshell diameter was increased from 10 m to 12 m to maintain the fixed packing density and a ballistic coefficient below 400 kg/m^2. The increased diameter of the aeroshell does not allow for the vehicle to fit into the fairing of any existing or planned launch vehicle, requiring on-orbit assembly of both the aeroshell primary structure and TPS. Even with the added complication of on-orbit assembly and integration, the benefit of gaining drag area and volume by increasing the aeroshell diameter was concluded to be acceptable.

Attached Inflatable Aerodynamic Decelerators

An IAD is a deployable, mass-efficient device to increase the drag area an entry vehicle for decelerating from supersonic to subsonic conditions. Early investigation of attached IADs was directed towards an Earth entry vehicle operating within the flight envelope of Apollo, with deployment at or below Mach 3 and dynamic pressures above 5000 Pa [9]. For application to Mars EDL, it was of interest to investigate the use of attached IADs at higher Mach numbers and lower dynamic pressures. Small-scale experimental work in the 1960s demonstrated the successful deployment of an attached IAD at dynamic pressures up to 5750 Pa at Mach 3 and as high as Mach 4.4 at a dynamic pressure of 3500 Pa [10]. Limitations on the deployment conditions are based on the materials response and structural integrity of the IAD, unlike supersonic parachutes, which are primarily limited by stability and aerodynamic drag performance [11]. An attached IAD was selected for its superior aerodynamic performance and stability at high supersonic Mach numbers, providing a drag coefficient up to 50% greater than a similar towed decelerator at conditions between Mach 5 and Mach 2 [9].

While IAD technology looks promising for future missions, challenges associated with fabrication, deployment, scalability, and questions about just how large of an IAD is feasible are currently active areas of research [10],[11]. Preliminary aerodynamic calculations indicate that an attached IAD designed to decelerate a 20 t payload at Mars is likely to be between 25 and 30 m in diameter, systems more than an order of magnitude larger in diameter than any IAD tested to date. Additional difficulty remains in where and how to test under Mars-relevant conditions, likely requiring a flight test and qualification program comparable to the Viking BLDT program in the 1970s. An attached IAD has the potential to be a lightweight, efficient alternative to supersonic retropropulsion to increase payload mass to the surface of Mars once the material technology, required testing, and flight performance are better

understood. For the potential mass advantage of a deployable aerodynamic decelerator over a purely propulsive descent, a 30 m diameter attached IAD, deployed at Mach 5 and used until Mach 2 has been baselined in this study.

Supersonic Retropropulsion

Supersonic retropropulsion, while never flown, was explored extensively in the 1960s and 1970s for application to planetary EDL as a supersonic decelerator [12]. The experimental work during this time yielded that supersonic retropropulsion, in a configuration with the nozzles at the periphery of the vehicle, could provide propulsive deceleration while maintaining the aerodynamic drag of the blunt body aeroshell, an effect not observed in the subsonic case [12]. The peripheral retropropulsion configuration prevents the portion of the bow shock over the vehicle nose from being disturbed by the nozzle exhaust for low to moderate thrust effort, maintaining a region of high pressure inboard of the nozzles, preserving the vehicle's aerodynamic drag. One test series suggests the possibility of even augmenting the aerodynamic drag by flattening the edges of the bow shock to have the freestream essentially see a drag area larger than the actual vehicle [12].

With less reliance on aerodynamic performance to provide deceleration and fewer challenges in manufacturing and scalability than IADs or parachutes, the maturation and use of supersonic propulsion for Mars EDL is highly feasible in the next 10-15 years as robotic precursor and human surface missions are conceptualized in greater detail. Testing in ground facilities can be done with subscale models, as previous experimental work shows excellent agreement between blunt body configurations of various scale. As with most EDL component testing in ground facilities, not all environmental conditions can be matched. While this technology has a greater mass benefit for payload masses greater than 20 t, supersonic retropropulsion has been included in this concept primarily due to the significant uncertainties in developing and qualifying alternate supersonic aerodynamic decelerator technologies.

Supersonic and Subsonic Parachutes

To date, all successful Mars missions have used a supersonic disk-gap-band (DGB) parachute to decelerate the entry vehicle to a subsonic terminal velocity, enable the jettison of a heatshield, and provide stability through the transonic regime [1]. While both supersonic and subsonic parachutes were considered in this study, parachutes were found to have no feasible application in the final design, replaced by alternative supersonic decelerator technologies and a fully propulsive subsonic terminal descent.

Supersonic Parachutes

MSL is challenging the performance and qualification limits of the supersonic DGB parachute, flying the largest parachute ever on another planet at 21.5 m in diameter. As payload masses increase, higher deployment Mach numbers and dynamic pressures are required to provide the necessary timeline for transition to terminal descent and landing. While existing parachute materials place an upper limit on deployment at Mach 2.7 – 3.0 [1], the drag performance and stability of the parachute degrade rapidly as the deployment Mach number increases above Mach 2.3, precluding a decision to extend the deployment conditions and parachute diameter for a 20 t payload.

To approximate the diameter for a supersonic DGB parachute to decelerate an 80 t entry vehicle from Mach 3 to 50 m/s, a diameter was interpolated from data for 100 t (130 m diameter) and 50 t (90 m diameter) entry masses [1]. The 80 t vehicle used in this case would require a 114 m diameter parachute, a dimension unrealistic in terms of inflation time, fabrication, and testing. While IADs share similar problems with fabrication, inflation time, and testing, the need for a decelerator at Mach numbers above Mach 3 without degrading drag performance with increasing Mach number led to the selection of an attached IAD for the baseline configuration over a supersonic parachute.

Subsonic Parachutes

Heritage EDL systems typically stage to a subsonic parachute to keep the aeroshell stable at subsonic velocities and remove the last remaining energy of the entry vehicle in preparation for landing. A study for an 1800 kg payload, 4.57 m diameter aeroshell, and landed altitude of +2.5 km MOLA required subsonic parachute diameters between 43.1 m and 57.2 m [2]. This study has a payload mass of 20 t, requiring an impractical or infeasible subsonic parachute drag area. While this dimension could be reduced by a staged or clustered system, the complexity of such a system of subsonic parachutes poses an additional failure potential and would be difficult or impossible to test and qualify on Earth. Accordingly, the subsonic descent and landing phase in this study are purely propulsive.

Skycrane / Landing Gear

The rugged Martian topography, particularly in regions of scientific interest, requires lander missions to have a shock attenuation system. Additionally, the thin atmosphere and size of the payload require propulsive terminal descent, resulting in significant interaction of the exhaust plumes with the ground. Four types of landing systems have been designed to handle these challenges at Mars: crushable legs (Viking, Phoenix), airbags (Mars Pathfinder (MPF), MER), a skycrane (MSL), and pallet landing gear [13].

The multi-legged crushable landing gear is flight proven from Viking and Phoenix. However, the landing gear leaves the payload suspended up to several meters above the ground and is susceptible to failure if one of the legs catches on a nearby rock during touchdown. Airbags, while successfully used on MPF and MER, are complex and fragile, with a high risk of failure if the release conditions are slightly off-nominal. The pallet system deploys cable-stayed outriggers, or legs, to increase its footprint and keep the payload closer to the ground. Each leg has a degree of freedom to rotate about its fixed "knee" when contact is made with the ground, and upon doing so they each pull attached cables through hollow deformable tubes. The system is capable of landing on terrain up to 30° in slope with a 1 m hazard clearance and vertical and horizontal velocities of 4 m/s and 2 m/s, respectively [13]. The skycrane will be flown for the first time on MSL, though the bridle system has heritage from MER. While propulsively expensive, the skycrane places the payload directly on the surface and has limited hazard avoidance, capabilities unique among the mentioned landing systems.

This configuration uses a combination of the skycrane and the pallet landing system. The propulsion system for the skycrane is the same throttleable system in the backshell used for supersonic and terminal descent. This combination allows for a controlled descent rate, avoids problems of plume interaction with the ground and the payload, and provides the ability to touchdown away from crippling terrain hazards at the target landing site. The inclusion of the pallet landing gear allows for a minimum descent rate of 2.4 m/s and places the payload closer to the ground than traditional landing gear. A comparison of the EDL configuration presented in this study to Viking, MER, and MSL is given in Table 2 below.

Table 2: Comparison with Other Mars Robotic Missions [1]

	Viking	MER	MSL	This Study
Entry Mass (kg)	992	~830	3600	75516
Aeroshell Diameter (m)	3.5	2.65	4.5	12.05
Packing Density (kg/m^3)	118.5	235.5	187	150
Ballistic Coefficient (kg/m^2)	64	94	142	390.3
L/D_{max}	0.18	0	0.24	0.2
Peak Heat Rate (W/cm^2)	26	44	136	1200
3σ Error Ellipse Major Axis (km)	280	80	12.5	1
Landing Site Elevation (km MOLA)	-3.5	-1.4	1	0

EDL MODEL

Atmosphere Model

The atmosphere model was developed by Seiff [17] following the Viking and Mars 6 missions in the 1970s. The model is given in the reference as tabulated data for temperature, pressure, density, and gravitational acceleration as a function of altitude, up to 100 km. The Seiff atmosphere model used is for the northern hemisphere in the summer season at latitudes below 60º. The surface density at 0 km is 1.56×10^{-2} kg/m^3. All atmosphere conditions at altitudes below 0 km are assumed to be equivalent to conditions at 0 km. 0 km is defined relative to the Mars reference ellipsoid developed by Christensen in 1975 [18]. The surface conditions (conditions given for 0 km) were determined by translating surface measurements from Viking 1 (-1.5 km), Viking 2 (-2.5 km), and Mars 6 (+1.3 km) to equivalent conditions on the reference ellipsoid.

Seiff also includes a characterization of cool and warm models for the summer season, which vary from the nominal model by ±10 K. For the cool model, the surface pressure is set to the minimum measured surface pressure from the Viking landers. For the warm model, the surface pressure is set to the maximum. The resulting density profiles differ from the nominal atmosphere by approximately 5% near the surface and 50% at high altitude. The cool and warm atmospheres are tabulated every 4 km, up to 100 km. These off-nominal atmospheres are used to develop the atmospheric dispersions applied in the Monte Carlo analysis.

Trajectory Model

All trajectory analysis was completed using an independently developed MATLAB-based 3-DOF tool. The equations of motion assume a spherical, non-rotating Mars and a point mass for the entry vehicle. Atmospheric interface is defined at 120 km altitude. Two velocities are defined, one with respect to the planet surface and one with respect to the atmosphere, allowing wind effects to be included in the planar direction integration. Both vectors are defined in a planet-centric frame, with the z-axis in the radial direction and the x-axis such that the velocity with respect to the planet is always in the xz-plane. Wind velocity is assumed to lie only in the xy-plane [14]. Aerodynamic forces are relative to the vehicle-sensed atmosphere and are independent of the planet surface.

To run the trajectory model, the simulation requires initial trajectory and state conditions of mass, velocity, altitude, and flight path angle. A simulation time span is input, as well as specification of event termination conditions and a desired downrange target for the hypersonic guidance algorithm. The model is capable of halting at a specific altitude, Mach number, and at deployment or jettison events. The trajectory code outputs the integrated parameters specified in the initial conditions as functions of time for the entire trajectory.

The stagnation point heating profile is generated using the Sutton-Graves stagnation point convective heat rate relation with the Mars-specific constant 1.9027×10^{-4} $(kg/m^3)^{1/2}$ [15]. This approximation assumes purely convective, laminar heating and the effective nose radius to be nearly equal to the geometric nose radius. The total integrated heat load is approximated using trapezoidal integration of the heat rate over time. Radiative heating is estimated from an analytic expression developed by Tauber and Sutton [16]. However, the velocities at which the vehicle performs aerocapture remain consistently below 6 km/s, and combined with low densities in the range of altitudes considered (30 – 100km), the resulting radiative heat rate represents only 1% of the total heat rate and is neglected in most cases.

Hypersonic Active Guidance

In the nominal simulation, a constant bank angle of 45° throughout the entry results in initiation of the terminal descent phase at 1949 km downrange and 4.21 km altitude. An active "predictor-corrector" hypersonic guidance algorithm was implemented to correct any deviations from the nominal trajectory resulting from uncertainties in the vehicle state and atmospheric conditions. Every 50 seconds, the guidance algorithm assesses the current vehicle state and simulates the remaining portion of the trajectory with a nominal, no wind atmosphere through to landing with bank angles varying from 0 to 75° at 15° increments. The algorithm then commands the best bank angle until the next update 50 seconds later, evaluating the highest bank angles first. For trajectories falling short of the downrange target without a bank angle change, the algorithm detects the energy deficit early in the trajectory and adjusts accordingly.

Supersonic Deceleration

Attached IAD

An IAD is deployed when the vehicle enters a "Mach-q box" bounded by Mach 5.0 and a dynamic pressure of 4000 Pa. Inflation of the IAD was assumed to occur instantaneously in this analysis and any instabilities and residual oscillations associated with the deployment have also been neglected. The attached IAD is used until the vehicle decelerates to Mach 2, at which point, the IAD is jettisoned.

Supersonic Retropropulsion

At Mach 2, the retropropulsion phase is initiated and decelerates the vehicle to Mach 0.9, the condition for the initiation of the terminal guidance algorithm. The model applies the aero-propulsive effect of increased drag area caused by firing the 6 retronozzles in the backshell into the opposing freestream. The assumed increase in effective drag area due to preservation of the blunt body aerodynamic drag is a factor of 3, aggressively based on experimental data for a similar retropropulsion configuration [12]. A constant thrust magnitude of 300 kN, assumed to act directly opposite the vehicle velocity, is used in this phase, evenly divided between the 6 engines. The configuration of engines at the aeroshell periphery causes the vehicle to tend toward its axisymmetric trim angle of attack at 0º.

Terminal Descent and Guidance

The terminal descent is composed of two phases: approach and vertical descent. Approach begins at the end of the supersonic retropropulsion phase at Mach 0.9 and ends at an altitude of 30 m above the landing target. At this point, the vehicle transitions from approach to vertical descent with the skycrane. The propulsive stage of the skycrane remains at a constant altitude 30 m while the payload is lowered on bridles to the surface at a constant rate of 2.4 m/s.

Approach Phase

The algorithm employed during the approach phase is an optimal guidance algorithm by D'Souza for planetary landing [20]. The feedback control law relates the required thrust to the state vector and the remaining time at every point along the trajectory. This algorithm avoids problems of sensitivity to initial guesses characteristic of two-point boundary value problems by using an analytically derived expression of the control law.

The terminal descent constraints are a final altitude of 30 m, a final velocity magnitude of 0 m/s, a required propellant mass less than 9000 kg, and a maximum thrust magnitude less than 500 kN. Within the specified tolerance (1×10^{-7}), the guidance algorithm converges to the target every time. However, the solutions found in this study are considered feasible only if the propellant mass and maximum thrust constraints have not been violated.

The required thrust magnitude is between 255 and 345 kN and is maximized at both the start and end of the approach phase, as shown in Figure 8. Without weighting the total time of the descent, the first trajectory selected by the algorithm does not stop 30 m above the surface. Increasing the weighting parameter to prevent violation of the altitude constraint forces the vehicle to reach the target more quickly with a higher initial downrange velocity.

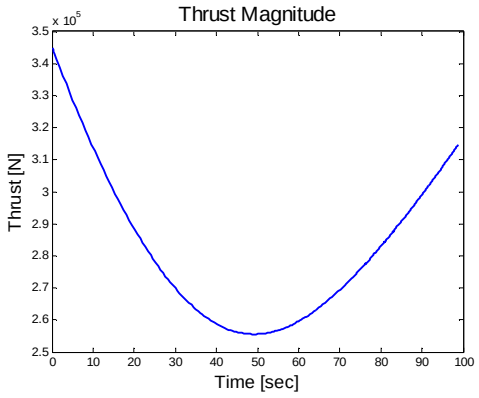

Figure 8: Nominal Terminal Descent Thrust Profile

Vertical Descent

At the end of the approach phase, the vehicle begins lowering the payload out of the backshell to the surface. Assuming the skycrane platform remains a constant 30 m above the ground, the skycrane – lander system is modeled in static equilibrium. The lander descends and touches down at 2.4 m/s, a rate similar to past Mars missions utilizing landing gear [1]. Due to the height of the payload with the landing gear deployed (5.3 m), the actual descent height is only 24.7 m, corresponding to a vertical descent time of 10.3 seconds. Once the lander reaches the surface, the bridles are cut, and the propulsive stage flies away. A 15% margin is applied to the entire propellant mass, providing the skycrane with the capability to crash at a safe distance away from the payload.

DISPERSION ANALYSIS

A first-order Monte Carlo analysis was performed to demonstrate the robustness of the nominal trajectory and EDL system configuration. Dispersions were applied to the vehicle's initial state, atmospheric conditions, and winds. In the analysis, the entry flight path angle was varied using a normal distribution, with a mean at the nominal entry value and a 3σ value of 0.04°. Dispersions to the initial vehicle state assumed a 2% accuracy of the deorbit burn, resulting in a maximum entry flight path angle variation of 0.03° and a maximum velocity variation of 20 m/s.

The atmospheric temperature and density profiles were varied over the ranges for the low and high pressure atmospheres specified by Seiff [17]. For the low pressure atmosphere, the density is ~ 5% less than the nominal atmosphere near the surface and ~ 50% less than the nominal near the edge of the atmosphere. The high pressure atmosphere is similar, with the density ~ 5% higher near the surface and ~ 50% higher in the upper atmosphere. The density profile is normally distributed about the nominal profile. The 3σ value was normalized to ±1, with any value generated outside those bounds reset to the nearest boundary.

The vehicle was also subjected to dispersions in wind velocity and direction. Winds on Mars can be as high as 140 m/s near the 60°N latitude line [5]. However for the 11°N maximum latitude of interest for the descent profile, the winds are significantly less, on the order of 20 m/s. Also, surface winds remain under 20 m/s with 99% confidence across the entire planet. Under these conditions, the wind was assumed to vary uniformly over a range of 0 to 20 m/s. The wind direction was uniformly dispersed, allowing for the wind vector to act in any direction in the xy-plane.

In the hypersonic phase, out-of-plane wind effects were assumed to be negligible. The lifting body is capable of mitigating the effect of small side forces due to the wind through biased bank angle modulation. A heading change on the order of 0.1° can compensate for kilometers of wind-induced crossrange error. Wind effects during terminal descent were accounted for both in-plane and out-of-plane.

With these dispersions, 800 entry cases were simulated to demonstrate the robustness of the entry vehicle design to entry state errors, atmospheric variability, and winds. The Monte Carlo analysis was performed from the entry interface to Mach 0.9, the condition for terminal guidance initiation. Final conditions, including altitude and downrange, values were logged, and the extremes of the dispersions were passed to the terminal guidance algorithm to demonstrate a valid descent and landing.

More than 99% of the cases reached Mach 0.9 conditions, allowing the terminal descent guidance algorithm to safely land the vehicle within the desired footprint without exceeding the propellant and thrust limits. Figure 9 shows the altitude and downrange for each case at terminal guidance start. The terminal descent guidance algorithm targets a distance 15 km downrange from terminal descent engage. The cases marked by squares all reached the target landing site, indicated by the triangle, without exceeding maximum thrust or propellant usage constraints. The cases marked by diamonds and outside of the highlighted terminal descent corridor failed to meet one of these two constraints during terminal descent.

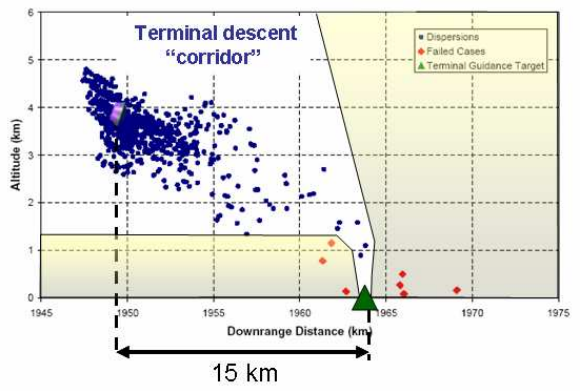

Figure 9: Terminal Descent Initiation Conditions for all 800 Cases

The cases that overflew the target in downrange and did not reach Mach 0.9 above 1 km MOLA were cases flying through a high density atmosphere coupled with large dispersions on entry flight path angle and winds. With the increased density, the dynamic pressure at Mach 5.0 exceeded the maximum allowable dynamic pressure for IAD deployment. If the guidance algorithm predicts IAD deploy at Mach 5.0, and the actual deploy does not occur until later, the vehicle loses significant altitude and gains significant downrange distance prior to initiation of the terminal descent phase. The resulting landing accuracy, with the selected dispersions, is 99.13%.

VEHICLE SIZING

It was assumed that prior to aerocapture that avionics, communication, and power are provided by a service module or transit stage as specified by ESAS / DRM [22],[23]. Following separation of the entry vehicle from the transit stage, the entry vehicle is dependent on the communications and avionics hardware in the payload. Aggressive growth margins of 20% and 15% were applied to the vehicle dry mass, including the payload, and the required propellant mass respectively. The resulting payload mass fraction is approximately 30%. The detailed mass breakdown is given in Table 1.

Propulsion

The propulsion system for EDL uses a total of 8 LOX/CH_4 engines, with two engines for aerocapture and on-orbit maneuvers and six engines for propulsive deceleration and terminal descent. LOX/CH_4 is the baseline as these systems are being developed for lunar and Mars exploration missions, both human and robotic. The engine sizing assumes an I_{sp} of 350 seconds [22],[23]. The engine dry mass is calculated from a regression analysis for conceptual LOX/CH_4 engines from thrust vs. mass data [22]. The total mass of the propulsion system includes propellant required for aerocapture maneuvers, supersonic retropropulsion, terminal descent, and the skycrane landing sequence, as well as insulated fuel and oxidizer tanks and engine dry mass. Total propulsion system mass is 2208 kg, including propellant.

IAD

The mass for the 30 m diameter attached IAD is estimated using a structural merit function developed by Anderson, Bohon, and Mikulas [25] for aerodynamic decelerators. The merit function relates structural and aerodynamic performance parameters to determine the relative decelerator efficiency. Using this merit function, the mass of the IAD, including fabric and structure is 1130 kg. The gas generator for deployment is sized to the dynamic pressure required at deployment conditions, and when combined with the storage structure for the IAD, the supplementary systems total 1017 kg. The total IAD system mass is 2147 kg.

TPS

In place of performing a 1-D heat transfer analysis, the TPS sizing relied on a historical mass estimating relation based on the integrated heat load, shown in Figure 10. The historical data is from ablative TPS designs for Viking, MPF, and MER. As this concept has two atmospheric phases, two separate heatshields are used, with the aerocapture heatshield jettisoned after the circularization maneuver. The mass estimates given in Table 1 include both the TPS material and the underlying structure, with the potential need for ballast absorbed into a global margin on the vehicle dry mass.

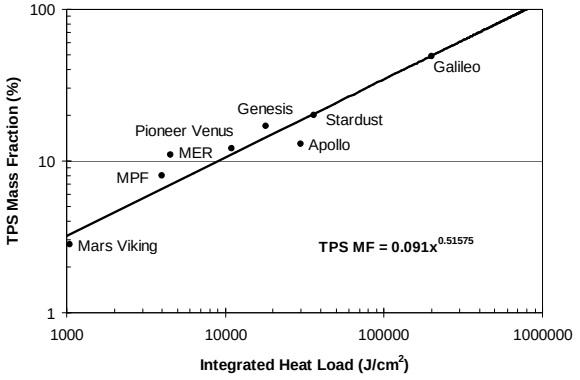

Figure 10: Historical TPS Mass Fractions

Recent aerothermodynamic studies for the MSL entry vehicle, including flight environment uncertainties, predict a stagnation point integrated heat load of 2300 J/cm^2. For the 70° sphere cone aeroshell geometry and

relatively high angle of attack (~15°), the leeward shoulder experiences much higher heat loads than the nose, on the order of 6500 J/cm^2 as compared to 2300 J/cm^2 at the nose. A scaling relationship adapted from the MSL configuration to this concept shows the integrated heat loads for this design are likely to reach values of the order of 15000 J/cm^2 [27].

The high angle of attack moves the stagnation point and augments turbulent flow transition, resulting in an increase in heating, possibly exacerbated by the existence of heatshield gaps [28]. Transient localized heating due to RCS interactions caused by the bank angle modulation maneuvers also exists and contributes to heating on the backshell. All these effects combined support the selection of honeycomb-packed SLA-561V on the backshell as well as the forebody, instead of a spray-on version. A linear regression using heritage values of peak heat load [1] suggests that the required aerocapture heatshield TPS thickness, using SLA-561V, is approximately 4.09 cm. While recent testing and analysis has raised concerns with the performance of SLA-561V, the material performance was not in question at the time of this study.

The specification of an ablative TPS material was made by comparison to MSL and prior Mars robotic missions, the aerothermal environment experienced during EDL, and the lack of a requirement for reusability. As mentioned above, SLA-561V is the baseline TPS material for the concept developed in this study, though other candidate materials such as PICA are likely better suited for the expected aerothermal environment. PICA was not sized in this case. The inability to manufacture a single piece of these materials large enough to cover the entire aeroshell base area will require panels of the material to be integrated in sections [24]. The uncertainty of the effect of gaps between the sections and the difficulty in integrating these sections has not been considered here. The TPS mass fraction for aerocapture is 9%, and the TPS mass fraction for the subsequent entry from a 200 km parking orbit is 7%. Comparing with Figure 10, these mass fractions agree with those from historical missions, considering all missions except Viking used a direct entry, experiencing higher heating conditions than those for aerocapture.

Power

Prior to aerocapture, the entry vehicle separates from the transit stage and begins to power the necessary EDL systems from onboard lithium-ion batteries. The mass estimate given in Table 1 includes the batteries, wiring harness, power control units, regulators, and converters. Assuming a conservative power density of 0.15 kW-hr/kg and a 3 kW total power allotment with margin, the Li-ion batteries can support the entry vehicle for a maximum of 12 hours between separation from the transit vehicle and power-up of the payload on the surface.

Avionics and Communications

The avionics and communications system is assumed to be similar to the systems specified for MSL. Included is hardware for command, control, data handing, guidance, navigation, communications, tracking, and spacecraft health monitoring [23]. An X-band radio system with one high-gain and two-low gain antenna was assumed to be aboard the spacecraft to utilize the Deep Space Network for communication with Earth [22]. By percentage, the mass allocated for avionics and communications is 0.8% of the vehicle dry mass.

Structures

The primary structure is estimated as an aggressive 12.5% of the vehicle dry mass, including the aeroshell, payload support structure, and mechanical systems for the skycrane, deployments, and jettison events. The pallet landing gear is sized as 1.2% of the dry mass [29].

CONCLUSIONS

Mars missions of the coming decades, both human and robotic, will require landed masses an order of magnitude greater than any Mars EDL mission to date. This study outlined a concept capable of delivering a 20 t payload to a landing site at 0 km MOLA in the northern hemisphere with a landed footprint no larger than 1 km. The design presented utilizes aerocapture, hypersonic guidance, an attached IAD, supersonic retropropulsion, terminal descent guidance, a skycrane, and pallet landing gear to achieve these goals. The combination of these technologies results in a landing accuracy of 99.13%.

Each element of the design addresses EDL challenges unique to Mars: the thin atmosphere, surface hazards, landing accuracy, and the cost and ability to develop and qualify new EDL technologies. Aerocapture reduces the peak heating and eliminates the propellant mass needed for propulsive orbit insertion. The aeroshell is a Viking-heritage 70° sphere cone. The attached IAD and supersonic retropropulsion, in tandem, decelerate the vehicle to subsonic conditions and increase the timeline for executing terminal descent and landing. The hypersonic guidance and terminal guidance deliver the payload to the selected landing site, even with significant dispersions applied to the atmosphere, winds, and entry conditions. Lastly, the skycrane provides limited hazard avoidance capability, and coupled with pallet landing gear, can deliver the payload safely on sloped and rugged terrain.

The concept presented in this study requires extensive cost and long-term planning to develop. Viking-heritage EDL systems will be operating at, or even exceeding, their qualifications for MSL, reaffirming the need for new EDL technologies. This study recommends the development of more robust guidance algorithms, aerocapture, IADs and supersonic retropropulsion, the qualification of new and existing TPS materials at higher heat rates, and on-orbit assembly. While this collection of technologies is extensive, their development is imperative in enabling the next phases of Mars exploration.

REFERENCES

[1] Braun, R., Manning, R., "Mars Exploration Entry, Descent, and Landing Challenges," *Journal of Spacecraft and Rockets*, Vol. 44, No. 2, March-April 2007, p. 310-323.

[2] Cruz, J., Cianciolo, A., Powell, R., Simonsen, L., Tolson, R., "Entry, Descent, and Landing Technology Concept Trade Study for Increasing Payload Mass to the Surface of Mars," 4th International Symposium on Atmospheric Reentry Vehicles and Systems, Arcachon, France, March 2005.

[3] Wolf, A., Graves, C., Powell, R., Johnson, W., "Systems for Pinpoint Landing at Mars," *Advances in the Astronautical Sciences*, Vol. 119, Jan. 2005, pp 2677-2696.

[4] Wolf, A., Tooley, J., Ploen S., Ivanov, M., Acikmese, B., Gromov, K., "Performance Trades for Mars Pinpoint Landing", 2006 IEEE Aerospace Conference, Big Sky, MT, IEEEAC 1661, March 2006.

[5] Kaplan, D., "Environment of Mars," NASA Technical Memorandum 100470, Houston, TX, 1988.

[6] Goddard Spaceflight Center, Topographic Map from the Mars Orbiter Laser Altimeter (MOLA). NASA, URL: http://ssed.gsfc.nasa.gov/tharsis/Mars_topography_from_MOLA/ [cited 15 March 2007].

[7] Hall, J., "An Overview of the Aerocapture Flight Test Experiment," AIAA Atmospheric Flight Mechanics Conference & Exhibit, Monterey, CA, AIAA 2002-4621, August 2002.

[8] Moss, J., Blanchard, R., Wilmoth, R., Braun, R., "Mars Pathfinder Rarefied Aerodynamics: Computations and Measurements," *Journal of Spacecraft and Rockets*, Vol. 36, No. 3, 1999, pp 330-339.

[9] Gillis, C., "Deployable Aerodynamic Decelerators for Space Missions," *Journal of Spacecraft and Rockets*, Vol. 6, No. 8, Aug. 1969, p.885 – 890.

[10] Bohon, H., Miserentino, R., "Attached Inflatable Decelerator (AID) Performance Evaluation and Mission-Application Study," Journal of Spacecraft and Rockets, Vol. 8, No. 9, Sep. 1971, p. 952 – 957.

[11] Guy, L., "Structural and Decelerator Design Options for Mars Entry," *Journal of Spacecraft and Rockets*, Vol. 6, No. 1, Jan. 1969, p.44 – 49.

[12] Korzun, A., Cruz, J., Braun, R., "A Survey of Supersonic Retropropulsion Technology for Mars Entry, Descent, and Landing, " 2008 IEEE Aerospace Conference, Big Sky, MT, IEEEAC 1246, March 2008.

[13] Graf, J., Thurman, S., Eisen, H., Rivellini, T., Sabahi, D., "Second Generation Mars Landed Missions," Jet Propulsion Laboratory/California Institute of Technology, Aerospace Conference, IEEE Proceedings, Vol. 1, 2001, pp 243-254.

[14] Regan, F., Anandakrishnan, S., Dynamics of Atmospheric Re-Entry, AIAA Education Series, Washington, D.C., 1993.

[15] Sutton, K., Graves, R., "A General Stagnation Point Convective Heating Equation for Arbitrary Gas Mixtures," NASA TR R-376, Washington, D.C., Nov. 1971.

[16] Tauber, M., Sutton, K., "Stagnation-Point Radiative Heating Relations for Earth and Mars Entries", J*ournal of Spacecraft*, Vol. 28, No. 1, 1991, pp. 40-42.

[17] Seiff, A., "Post-Viking Models for the Structure of the Summer Atmosphere of Mars," *Adv. Space Res*, Vol. 2, 1982, p. 3-17.

[18] Christensen, E.J., *Journal of Geophysics*, Vol. 80, 2909, 1975.

[19] Johnson, A., Klumpp, A., Collier, J., Wolf, A., "Lidar-Based Hazard Avoidance for Safe Landing on Mars", *Journal of Guidance, Control, and Dynamics*, 0731-5090 Vol. 25, No. 6, 2002, pp. 1091-1099.

[20] D'Souza, C., "An Optimal Guidance Law for Planetary Landing", *AIAA Guidance, Navigation and Control Directorate*, New Orleans, LA, paper AIAA-1997-3709, Aug. 1997.

[21] Smith, R., Mease, K., Bayard, D., Farless, D., "Aeromaneuvering in the Martian Atmosphere: Simulation-Based Analyses," *Journal of Spacecraft and Rockets*, Vol. 37, No. 1, 2000, pp. 139-142.

[22] Hoffman, S., Kaplan, D., "Human Exploration of Mars: The Reference Mission of the NASA Mars Exploration Study Team," NASA Special Publication 6107, July 1997.

[23] National Aeronautics and Space Administration, "NASA's Exploration Systems Architecture Study," NASA TM-2005-214062, November 2005.

[24] Christian, J., Manyapu, K., Wells, G., Lafleur, J., Verges, A., Braun, R., "Extension of Traditional Entry, Descent, and Landing Technologies for Human Mars Exploration," *Journal of Spacecraft and Rockets*, Vol. 45, No. 1, January – February 2008, pp. 130-141.

[25] Anderson, M., Bohon, H., Mikulas, M., "A Structural Merit Function for Aerodynamic Decelerators," NASA TN D-5535, Nov. 1969.

[26] Wells, G., Lafleur, J., Verges, A., Manyapu, K., Christian, J., Lewis, C., Braun, R., "Entry, Descent, and Landing Challenges of Human Mars Exploration," 29th Annual AAS Guidance and Control Conference, Breckenridge, CO, American Astronautical Society, AAS 06-072, Feb. 2006.

[27] Edquist, K., Dyakonov, A., Wright, M., Tang, C., "Aerothermodynamic Environments Definition for the Mars Science Laboratory Entry Capsule," 45th AIAA Aerospace Sciences Meeting and Exhibit, 8 - 11 January 2007, Reno, Nevada.

[28] Edquist, K., Liechty, D., Hollis, B., Alter, S., Loomis, M., "Aeroheating Environments for a Mars Smart Lander", *Journal of Spacecraft and Rockets*, Vol. 43, No. 2, Mar. 2006.

[29] Hofstetter, W., Weck, O., and Crawley, E., "Modular Building Blocks for Manned Spacecraft: A Case Study for Moon and Mars Landing Systems," INCOSE 2005 - Systems Engineering Symposium, Rochester, NY, July 2005.